Global Journal of Pure and Applied Mathematics.
ISSN 0973-1768 Volume 21, Number 3 (2025), pp. 565-583
©Research India Publications
https://dx.doi.org/10.37622/GJPAM/29.09.2026.565-583

An Analytical Study of Two-Fluid Flow in a Porous Inclined Channel

Mithilesh Kumar Mishra[1], **Deepak Kumar**[*2]

[1]*Department of Mathematics L.N.D.College Motihari (A Constituent Unit of Babasaheb Bhimrao Ambedkar Bihar University, Muzaffarpur), Bihar-845401, India.*
Email: mithileshmishra0194@gmail.com

[2]*Department of Mathematics L.N.D.College Motihari (A Constituent Unit of Babasaheb Bhimrao Ambedkar Bihar University, Muzaffarpur), Bihar-845401, India.*
E-mail: deepakmaths@yahoo.com

Abstract

In the present paper, pulsating two-fluid magnetohydrodynamic (MHD) flow in a parallel plate inclined channel is analyzed. The channel is partially filled with porous medium. The governing flow equations in both clear fluid and porous regions are solved analytically. The resulting expressions for velocity, mass flux, and shear stress are derived for both areas. The effects of various flow parameters on the velocity and shear stress are depicted through graph.

Keywords: Conducting fluid, Porous medium, Multiphase flow

2020 Mathematics Subject Classification : Primary: 76S05; Secondary: 76T06.

Nomenclature

g	Acceleration due to gravity	h	Ratio of the heights of the two regions ($\frac{h_2}{h_1}$)
h_1	Height of the region - II	h_2	Height of the region - I
α	Ratio of the densities ($\frac{\rho_1}{\rho_2}$)	β	Ratio of the viscosities ($\frac{\mu_1}{\mu_2}$)
μ_1	Viscosity of the fluid in Region-I	μ_2	Viscosity of the fluid in Region-II
ρ_1	Density of the fluid in Region-I	ρ_2	Density of the fluid in Region-II
K	Permeability of the porous medium	Fr	Fraud number ($\frac{u}{\sqrt{gh_1}}$)
M	Hartman number($B_0 h_1 \sqrt{\frac{\sigma}{\mu_1}}$)	R_i	Reynolds number($\frac{\rho_1 h_1 u}{\mu_i}$)
p	Pressure	u_i	Velocities in x - direction
σ	Electrical conductivity of the fluid	B_0	Strength of applied magnetic field
t	time	τ_i	Shear stresses at the plates
Q_i	Mass fluxes	ω	Frequency
ϕ	Angle of the channel with the horizontal	x, y	Space coordinates

[*]Corresponding author

1. INTRODUCTION

Two-fluid flow means the simultaneous flow of two immiscible fluids through a medium. The fluids may be liquid-liquid, liquid-gas or gas-gas. This type of flow occurs in natural and man-made systems, such as groundwater flows, petroleum engineering, chemical engineering, and nuclear engineering. The accurate prediction of multi-phase flow is essential in designing systems, such as pipelines, reactors, heat exchangers, and many multi-phase transport systems. Malashetty and Umavathi [1] analysed two-phase MHD flow and heat transfer in an inclined channel. They determine that the magnetic field plays a crucial role in the flow velocity and heat transfer. Ghosh and Debnath [2] investigated two-phase flow in an inclined porous channel using numerical techniques and observed that porosity of the medium and the inclination of the channel affect flow and heat transfer. The flow of two immiscible viscous fluids in a porous medium between parallel plates has been studied by Kumar and Agarwal [3]. Umavathi et al. [4] investigated unsteady oscillatory flow and heat transfer in a composite porous medium channel. The effects of porosity parameter, viscosity ratio, oscillation amplitude, etc, were presented graphically. Abbas et al.[5] explored magnetohydrodynamic two-phase flow and heat in an inclined channel with partial slip, demonstrating the impact of magnetic field and slip conditions on the flow behaviour. The flow of two-immiscible fluids in porous and nonporous channels has been analysed by Chamkha [6].Malashetty et al.[7] conducted a study on two-fluid flow and heat transfer in an inclined channel with both porous and clear fluid layers. The paper emphasised the effects of the inclination angle and porous medium properties on the flow and heat transfer process. Priya et al.[8] examined the effects of heat and mass transfer on MHD convective flow of immiscible fluid in a horizontal channel with chemical reaction and heat source. Malashetty and Leela [9] studied MHD flow and heat transfer in two-phase flow. The focused on the impact of magnetic field on the flow and heat transfer. Hanvey et al. [10] analysed MHD flow of incompressible fluid in the parallel plate channel with porous medium by applying an inclined magnetic field. Chamkha et al. [11] investigated oscillatory flow and heat transfer of two immiscible fluids in a chennel. They focused on how the oscillatory parameter influences the flow behavior. Umavathi et al. [12] studied convective magnetohydrodynamic two-fluid flow and heat transfer in an inclined channel. Hafeez et al.[13] examined the flow of viscous fluid between two parallel porous plates with bottom injection and top suction. Devi et al.[14] investigated heat transfer effects on oscillatory MHD flow in a porous channel with two immiscible fluids. Umavathi et al.[15] studied unsteady two-fluid flow and heat transfer in a horizontal channel. Fangfang Xie [16] presented numerical simulation of two-phase flow in an inclined channel. Yan [17] analysed computational analysis of

wall transpiration on mixed convection in a radial outward flow inside rotating ducts.

In this paper, we obtained analytical solutions for pulsating two-fluid flow in an inclined channel that is partially filled with porous material.

2. MATHEMATICAL FORMULATION

The flow under consideration is depicted in Figure 1. The flow of two immiscible fluids in a channel partially filled with a porous medium is considered. The domain is divided into two regions: the upper clear fluid region (Region-I) and the lower porous region (Region-II). The interface between the clear fluid and the porous medium is located at $y = 0$. The clear fluid occupies the space between $y = h_1$ and $y = h_2$, while the porous region lies between $y = 0$ and $y = h_1$. The co-ordinate system is defined with x axis horizontally and y axis vertically. The channel is inclined with an angle ϕ with the horizontal. A uniform magnetic field of strength B_o is applied along the y axis. The flow is driven by a pulsatile pressure gradient, and is considered laminar and fully developed. The pressure gradient is taken of the form;

$$-\frac{\partial p}{\partial x} = \left(\frac{\partial p}{\partial x}\right)_s + \left(\frac{\partial p}{\partial x}\right)_o e^{i\omega t},$$

where $\left(\frac{\partial p}{\partial x}\right)_s$ and $\left(\frac{\partial p}{\partial x}\right)_o$ denote magnitudes of the steady and oscillatory parts of the pressure gradient, while ω and t denote the frequency and time, respectively.

The conducting fluid is considered in Region-I, while the non-conducting fluid is taken in Region-II. The fluids in both regions are immiscible, meaning there is no mixing between them at any level. Therefore, separate constitutive equations for the flows in both regions may be considered. For example, mineral oils (used in electrical transformers and cooling systems) are non-conducting fluids, while water is conducting fluid. it is know fact that, in general, mineral oils and water do not mix. Since the presented model is general, any two immiscible fluids can be chosen. Assuming that the only non-zero component of velocity is the X-component, the governing flow equations in Regions-I and II, are as follows:

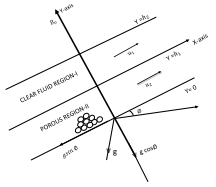

Figure 1: Flow diagram.

Region-I (Clear fluid region):

Equation of mass balance

$$\frac{\partial u_1}{\partial x} = 0, \tag{2.1}$$

Equation of momentum balance

$$\rho_1 \frac{\partial u_1}{\partial t} = -\frac{\partial p}{\partial x} + \mu_1 \frac{\partial^2 u_1}{\partial y^2} - \rho_1 g sin\phi - \sigma B_o^2 u_1. \tag{2.2}$$

Region-II (Porous region):

Equation of mass balance

$$\frac{\partial u_2}{\partial x} = 0, \tag{2.3}$$

Equation of momentum balance

$$\rho_2 \frac{\partial u_2}{\partial t} = -\frac{\partial p}{\partial x} + \mu_2 \frac{\partial^2 u_2}{\partial y^2} - \rho_2 g sin\phi - \frac{\mu_2}{K} u_2. \tag{2.4}$$

The velocities $u_1(y,t), u_2(y,t)$ satisfy the following boundary and interface conditions:

$$u_1 = 0 \qquad \text{at } y = h_2, \tag{2.5}$$

$$u_2 = 0 \qquad \text{at } y = 0, \tag{2.6}$$

$$u_1 = u_2 \qquad \text{at } y = h_1, \tag{2.7}$$

$$\mu_1 \frac{\partial u_1}{\partial y} = \mu_2 \frac{\partial u_2}{\partial y} \qquad \text{at } y = h_1. \tag{2.8}$$

The equations 2.5 and 2.6 represent no-slip conditions at the boundary, while the equations 2.7 and 2.8 represent matching conditions at the fluid-fluid interface. Since the fluids are immiscible, the matching conditions can be applied at the interface.

Since the pressure gradient is pulsatile, the velocities can be assumed to have a similar form.

$$u_i = u_{i1} + u_{i2} e^{i\omega t}\ , \qquad i = 1, 2,$$

where the steady and oscillatory parts of the velocities are u_{i1} and u_{i2}, respectively.

3. NON-DIMENSIONALISATION OF FLOW QUANTITIES

The following transformations are applied in order to make the governing equations and the boundary conditions dimensionless:

$$x^* = \frac{x}{h_1}, \quad y^* = \frac{y}{h_1}, \quad u_i^* = \frac{u_i}{u}, \quad u_{i1}^* = \frac{u_{i1}}{u}, u_{i2}^* = \frac{u_{i2}}{u}, \quad t^* = \frac{tu}{h_1}, \quad K^* = \frac{K}{h_1^2}, \quad \tau_i^* = \frac{\tau_i}{\rho u^2} \quad w^* = \frac{wh_1}{u}, \quad p^* = \frac{p}{\rho u^2}, \quad M = B_0 h_1 \sqrt{\frac{\sigma}{\mu_1}}, \quad R_i = \frac{\rho_i h_1 u}{\mu_i},$$
$$Fr^2 = \frac{u^2}{gh_1}.$$

After dropping the asterisk, the governing equations of motion $(2.2\&2.4)$ can be obtained by

$$\frac{\partial u_1}{\partial t} = -\frac{\partial p}{\partial x} + \frac{1}{R_1}\frac{\partial^2 u_1}{\partial y^2} - \frac{1}{Fr^2} sin\phi - \frac{M^2}{R_1} u_1, \tag{3.1}$$

$$\frac{\partial u_2}{\partial t} = -\alpha\frac{\partial p}{\partial x} + \frac{1}{R_2}\frac{\partial^2 u_2}{\partial y^2} - \frac{1}{Fr^2} sin\phi - \frac{1}{R_2 K} u_2. \tag{3.2}$$

Boundary and interface conditions are given by equations $(2.5 - 2.8)$ and can be expressed in the form of:

$$u_1 = 0 \qquad \text{at } y = h, \tag{3.3}$$

$$u_2 = 0 \qquad \text{at } y = 0, \tag{3.4}$$

$$u_1 = u_2 \qquad \text{at } y = 1, \tag{3.5}$$

$$\beta\frac{\partial u_1}{\partial y} = \frac{\partial u_2}{\partial y} \qquad \text{at } y = 1. \tag{3.6}$$

The velocity and pressure gradient can be expressed in non-dimensional form as follows:

$$u_i = u_{i1} + u_{i2} e^{iwt}, \qquad i = 1, 2,$$
$$-\frac{\partial p}{\partial x} = \left(\frac{\partial p}{\partial x}\right)_s + \left(\frac{\partial p}{\partial x}\right)_o e^{iwt}.$$

Separating steady and oscillatory parts of the equations $(3.1\&3.2)$, we have

3.1. Steady flow

The governing equations of steady flow are given by

$$\frac{1}{R_1}\frac{d^2 u_{11}}{dy^2} - \frac{1}{Fr^2} sin\phi - \frac{M^2}{R_1} u_{11} + P_s = 0, \tag{3.7}$$

$$\frac{1}{R_2}\frac{d^2 u_{21}}{dy^2} - \frac{1}{Fr^2} sin\phi - \frac{1}{KR_2} u_{21} + \alpha P_s = 0. \tag{3.8}$$

The boundary conditions to be satisfied by u_{i1} are:

$$\begin{aligned} u_{11} &= 0 \qquad \text{at } y = h, && (3.9)\\ u_{21} &= 0 \qquad \text{at } y = 0, && (3.10)\\ u_{11} &= u_{21} \qquad \text{at } y = 1, && (3.11)\\ \beta\frac{du_{11}}{dy} &= \frac{du_{21}}{dy} \qquad \text{at } y = 1. && (3.12) \end{aligned}$$

3.2. Oscillatory flow

The governing equations of oscillatory flow are given by

$$\begin{aligned} \frac{1}{R_1}\frac{d^2u_{12}}{dy^2} - \left(\frac{M^2}{R_1} + iw\right)u_{12} + P_o &= 0, && (3.13)\\ \frac{1}{R_2}\frac{d^2u_{22}}{dy^2} - \left(\frac{1}{KR_2} + iw\right)u_{22} + \alpha P_o &= 0. && (3.14) \end{aligned}$$

The boundary conditions to be satisfied by u_{i2} are:

$$\begin{aligned} u_{12} &= 0 \qquad \text{at } y = h, && (3.15)\\ u_{22} &= 0 \qquad \text{at } y = 0, && (3.16)\\ u_{12} &= u_{22} \qquad \text{at } y = 1, && (3.17)\\ \beta\frac{du_{12}}{dy} &= \frac{du_{22}}{dy} \qquad \text{at } y = 1. && (3.18) \end{aligned}$$

where $P_s = (\frac{\partial p}{\partial x})_s, P_o = (\frac{\partial p}{\partial x})_o$.

4. SOLUTION OF THE PROBLEM

4.1. Steady flow solution

The solution of the steady flow presented in section (3.1) is

$$\begin{aligned} u_{11}(y) &= C_1e^{My} + C_2e^{-My} - A_1 && (4.1)\\ u_{21}(y) &= C_3e^{-yA_2} + C_4e^{yA_2} - A_3 && (4.2) \end{aligned}$$

where $C_1, C_2, C_3, C_4, A_1, A_2$ and A_3 are given in the Appendix.

4.2. Oscillatory flow solution

The solution of the oscillatory flow presented in section (3.2) is

$$u_{12}(y) = C_5 e^{-A_4 y} + C_6 e^{A_4 y} + A_5 \tag{4.3}$$

$$u_{22}(y) = C_7 e^{-A_6 y} + C_8 e^{A_6 y} + A_7 \tag{4.4}$$

where $C_5, C_6, C_7, C_8, A_4, A_5, A_6$ and A_7 are given in the Appendix.

4.3. Pulsatile flow solution

The solution of pulsatile flow is given by

$$u_1 = u_{11} + u_{12} e^{i\omega t}, \qquad u_2 = u_{21} + u_{22} e^{i\omega t}$$

where u_{11}, u_{12}, u_{21}, and u_{21} are given in equations $(27 - 30)$.

4.4. Shear stress

The shear stress at upper and lower plates in non-dimensional form, respectively, are given as

$$\tau_1 = \frac{1}{R_1}\frac{\partial u_1}{\partial y} \qquad \text{at } y = h \tag{4.5}$$

$$\tau_2 = \frac{1}{R_2}\frac{\partial u_2}{\partial y} \qquad \text{at } y = 0 \tag{4.6}$$

4.5. Mass flux

The instantaneous mass fluxes in both the regions, respectively, are given as

$$Q_1 = \int_1^h u_{11} dy + \left[\int_1^h u_{12} dy\right] e^{iwt} \tag{4.7}$$

$$Q_2 = \int_0^1 u_{21} dy + \left[\int_0^1 u_{22} dy\right] e^{iwt} \tag{4.8}$$

5. RESULTS AND DISCUSSIONS

The variations in velocity and shear stress profiles with different flow parameters are depicted through graphs (Figures: 2 to 14) for $K = 0.5, \alpha = 0.8, \beta = 0.7, h = 2, M = 1, F_r = 2, R_1 = 1.8, R_2 = 2, P_s = 2, P_o = 2, \phi = 10, \omega = 5, t = 1$ except where the parameters vary.

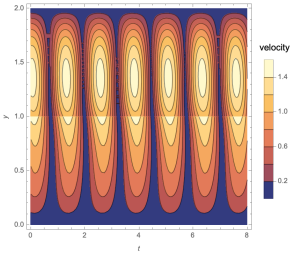

(a) Velocity profile at K=0.5

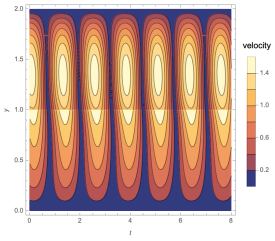

(b) Velocity profile at K=0.6

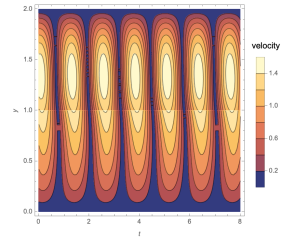

(c) Velocity profile at K=0.7

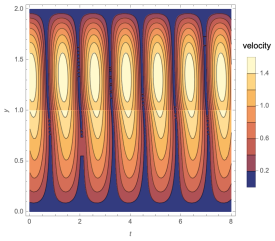

(d) Velocity profile at K=0.8

Figure 2: Velocity profiles with permeability

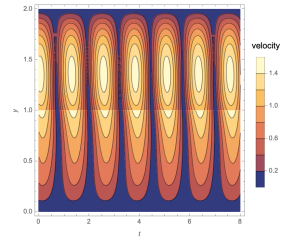

(a) Velocity profile at M=1

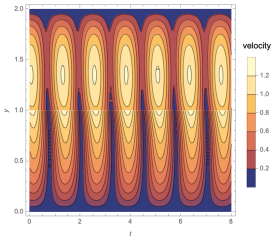

(b) Velocity profile at M=2

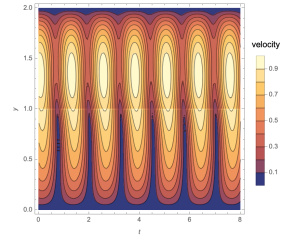

(c) Velocity profile at M=3

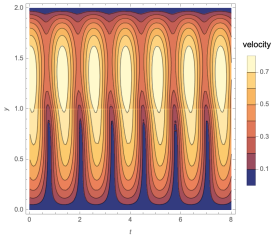

(d) Velocity profile at M=4

Figure 3: Velocity profiles with Hartmann number

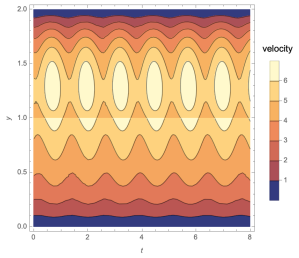

(a) Velocity profile at Fr=0.1

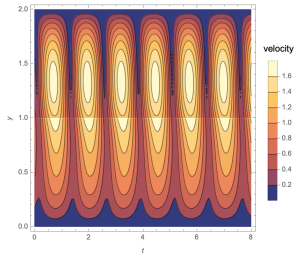

(b) Velocity profile at Fr=0.2

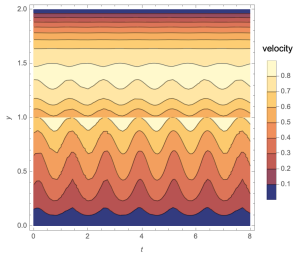

(c) Velocity profile at Fr=0.3

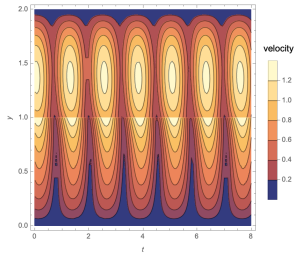

(d) Velocity profile at Fr=0.5

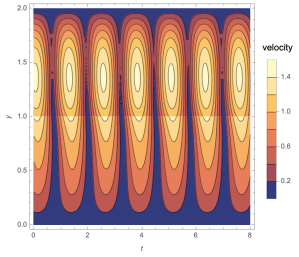

(e) Velocity profile at Fr=1

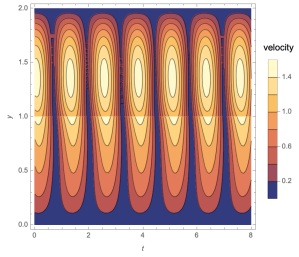

(f) Velocity profile at Fr=2

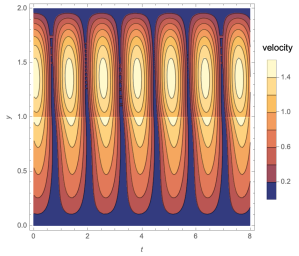

(g) Velocity profile at Fr=3

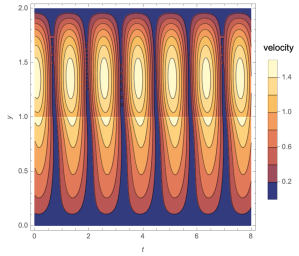

(h) Velocity profile at Fr=4

Figure 4: Velocity profiles with Froude Number

Figure 2 depicts velocity variations with respect to permeability of the porous medium. The velocity in Region-I increases, and the velocity in Region-II also increases due to the matching conditions at the interface. Figure 3 shows velocity changes relative to Hartman number. Velocity in both regions decreases with an increase in Hartmann number. An increase in Hartmann number leads to a stronger Lorentz force acting on the moving fluid, which opposes the fluid motion. Figure 4 depicts the velocity profile for Froude Number. An increase in Froude number leads to a decrease in the velocity in

both regions. As Fr increases from 0.1 to 0.3, the velocity decreases suddenly. Further increases in F_r from 0.3 to 4 lead to an increase in velocity. Figure 5 illustrates the changes in velocity with the inclination of the channel. The velocity decreases as the angle varies from 10^o to 55^o. This happens because flow is from a lower to a higher altitude. Figure 6 depicts the velocity profile with Permeability K (Figure 6a), Hartmann number M (Figure 6b), Froude Number F_r (Figure 6c), and inclination of the channel ϕ (Figure 6d). An increase in permeability results in an increase in velocity, while an increase in Hartmann number results in a decrease in velocity. An increase in the Froude number from 0.2 to 0.4 leads to a sudden decrease in velocity, while a further increase in the Froude number from 0.4 to 1 results in a gradual increase in velocity. Velocity gradually decreases for increase in angle of the channel from 10^o to 50^o. Figure 7 shows velocity variations for frequency ω (Figure 7a) and time t (Figure 7b) . Velocity exhibits mixed trends with both ω and t, as the motion is pulsatile.

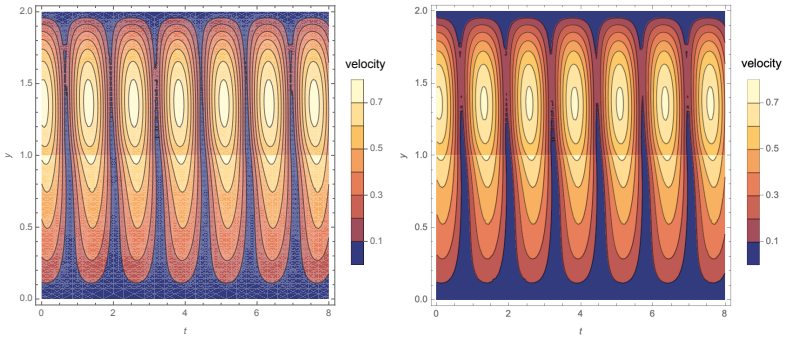

(a) Velocity profile at ϕ =10

(b) Velocity profile at ϕ =25

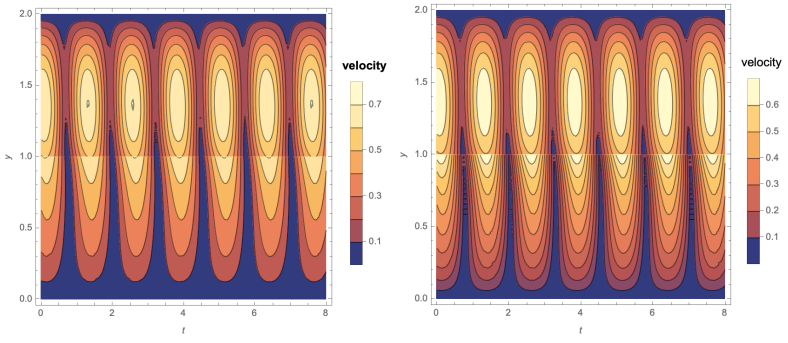

(c) Velocity profile at ϕ =40

(d) Velocity profile at ϕ =55

Figure 5: Velocity profiles with inclination of the channel

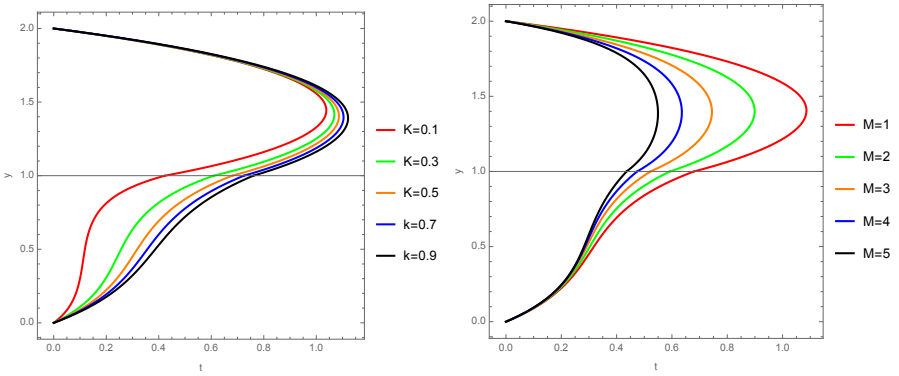

(a) Velocity variations with K (b) Velocity variations with M

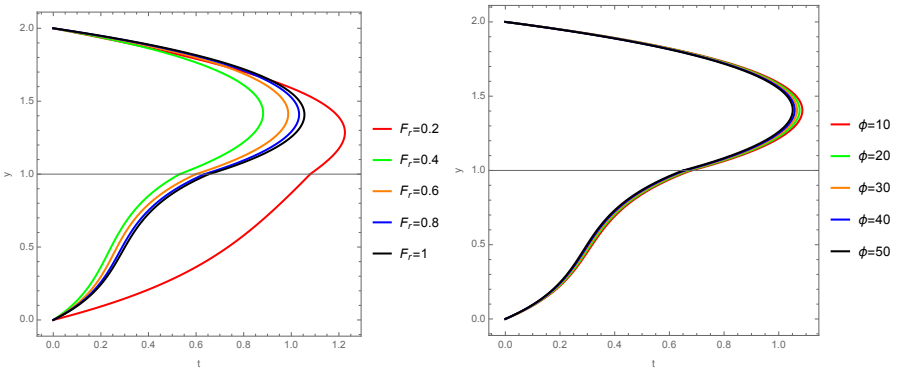

(c) Velocity variations with Fr (d) Velocity variations with ϕ

Figure 6: Velocity profiles at different flow parameters

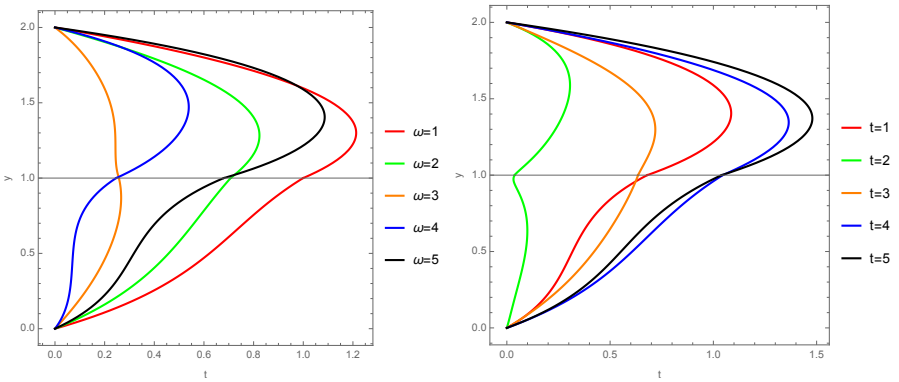

(a) Velocity variations with ω (b) Velocity variations with t

Figure 7: Velocity profiles at different flow parameters

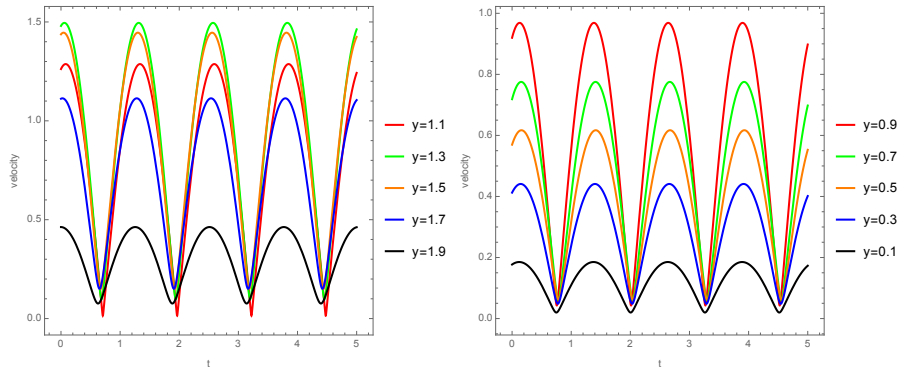

(a) Velocity variations in Region -I (b) Velocity variations in Region -II

Figure 8: Velocity profiles at different heights of the channel

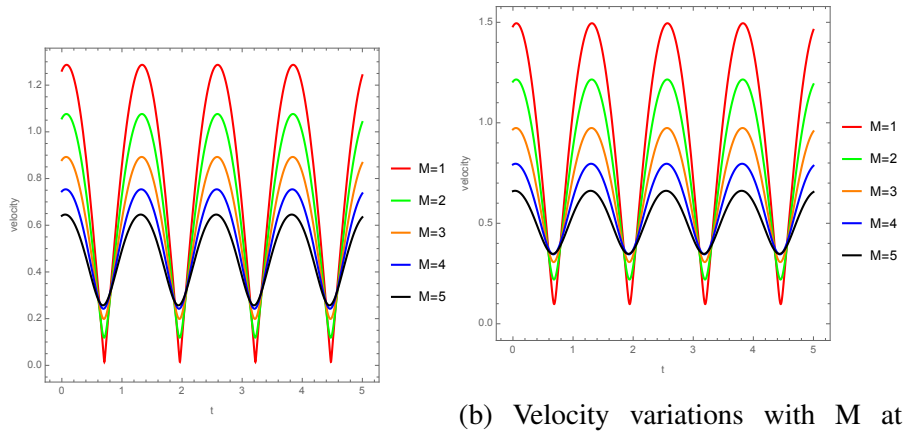

(a) Velocity variations with M at y=1.1 (b) Velocity variations with M at y=1.3

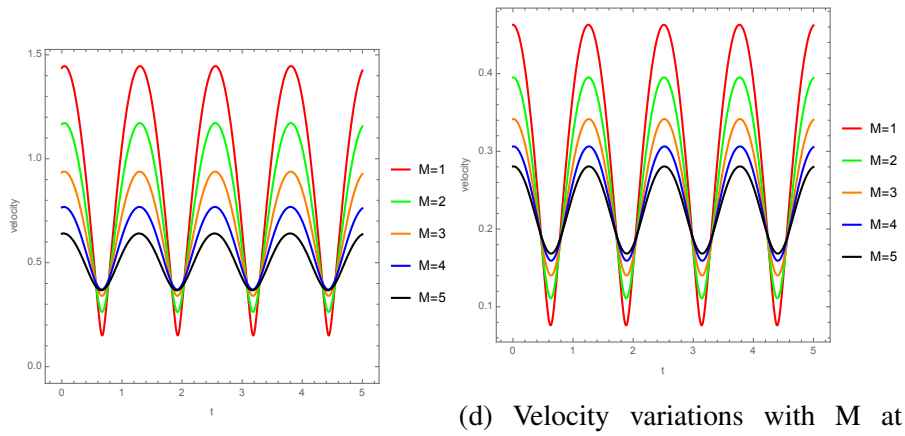

(c) Velocity variations with M at y=1.5 (d) Velocity variations with M at y=1.9

Figure 9: Velocity profiles for Hartmann number in Region -I

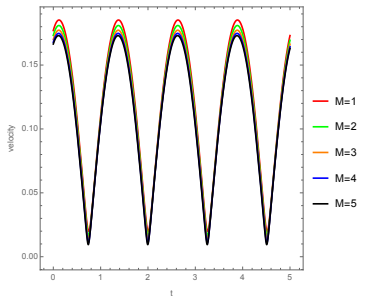

(a) Velocity variations with M at y=0.1

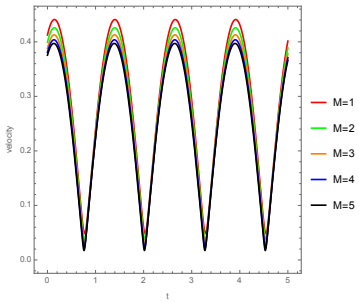

(b) Velocity variations with M at y=0.3

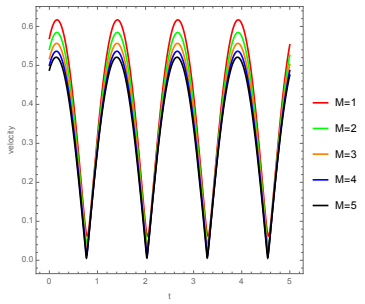

(c) Velocity variations with M at y=0.5

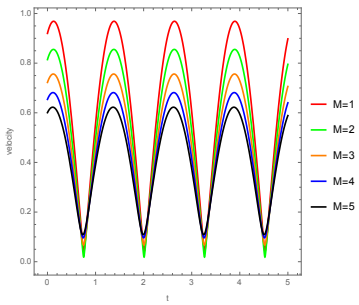

(d) Velocity variations with M at y=0.9

Figure 10: Velocity profiles for Hartmann number in Region -II

Figure 8 illustrates velocity profiles at different channel heights in Region-I (8a) and Region-II (8b). The velocity is maximum in the middle and minimum near the boundaries of the channel. Figures 9 and 10 depict the velocity profiles for different channel heights of Regions I and II, respectively, for the Hartmann number M. An increase in the Hartmann number results in a decrease in velocity in both Regions. Figures 11 and 12 represent the velocity profiles for different channel heights of Regions I and II, respectively, for the Froude number F_r . An increase in the Froude number from 0.1 to 0.3 leads to a sudden decrease in velocity, while a further increase in the Froude number from 0.3 to 0.9 results in a gradual increase in velocity. Figure 13 illustrates variations in the shear stress at the lower plate of the channel for the Froude number (Figure 13a), the Hartmann number (Figure 13b), permeability (Figure 13c), and inclination of the channel (Figure 13d). Shear stress at the lower plate first decreases rapidly, then gradually increases as the Froude number increases. As the Hartman number increases, shear stress at the lower plate decreases slowly. An increase in permeability of the porous medium leads to an increase in shear stress at the lower plate, while an increase in the inclination of the channel results in a decrease in shear stress at the lower plate. Figure 14 shows variations in the shear stress at the upper plate

of the channel for the Froude number (Figure 14a), the Hartmann number (Figure 14b), permeability (Figure 14c), and inclination of the channel (Figure 14d). Shear stress at the upper plate first decreases rapidly, then gradually increases as the Froude number increases. As the Hartman number increases, shear stress at the upper plate first decreases rapidly, then slowly. An increase in permeability of the porous medium leads to slow increase in shear stress at the upper plate, while an increase in the inclination of the channel results in a slow decrease in shear stress at the upper plate.

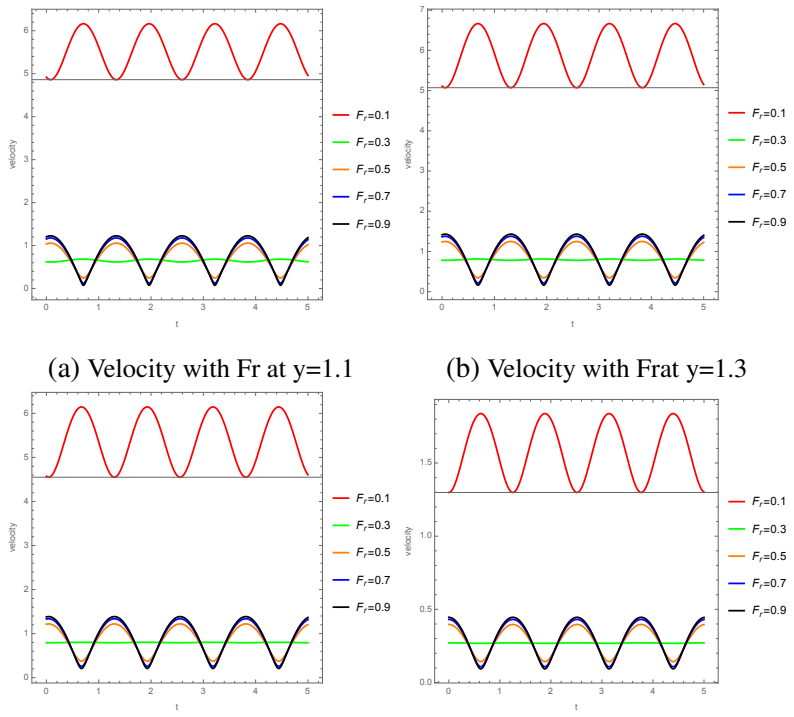

(a) Velocity with Fr at y=1.1 (b) Velocity with Frat y=1.3

(c) Velocity with Fr at y=1.5 (d) Velocity with Fr at y=1.9

Figure 11: Velocity profiles for Froude number in Region -I

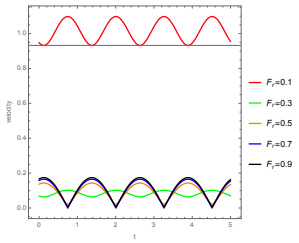

(a) Velocity with Fr at y=0.1

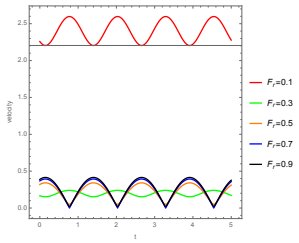

(b) Velocity with Frat y=0.3

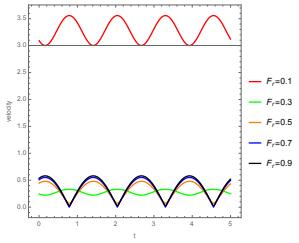

(c) Velocity with Fr at y=0.5

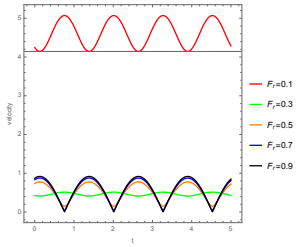

(d) Velocity with Fr at y=0.9

Figure 12: Velocity profiles for Froude number in Region -II

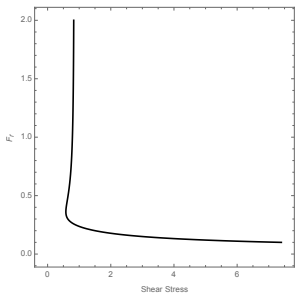

(a) Shear Stress at lower plate with Fr

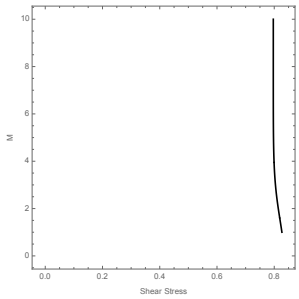

(b) Shear Stress at lower plate with M

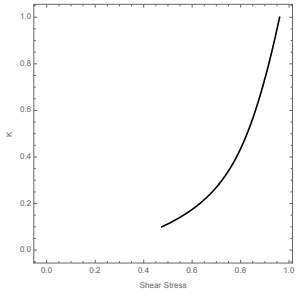

(c) Shear Stress at lower plate with K

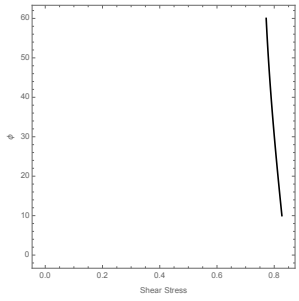

(d) Shear Stress at lower plate with ϕ

Figure 13: Shear stress at the lower plate

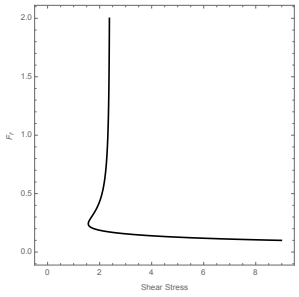

(a) Shear Stress at upper plate with Fr

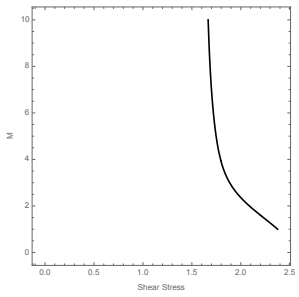

(b) Shear Stress at upper plate with M

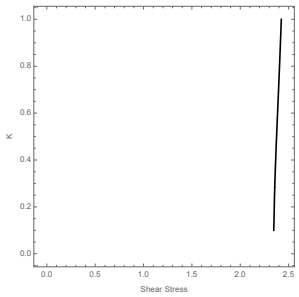

(c) Shear Stress at upper plate with K

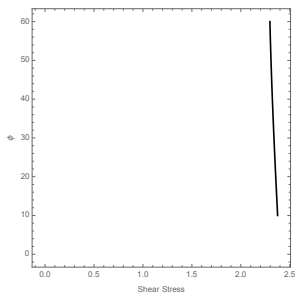

(d) Shear Stress at upper plate with ϕ

Figure 14: Shear stress at the upper plate

6. CONCLUSIONS

This paper presents an analysis of pulsating two-fluid MHD flow in a parallel plate inclined channel. The channel is partially filled with a porous medium. We obtained analytical solutions to the governing equations for flow in both the clear fluid and porous regions. The expressions for velocity, mass flux, and shear stress are derived in both the regions. Additionally, we illustrated the effect of various flow parameters on velocity and shear stress through graphs. The graphs display that:

- The Hartmann number opposes the flow, while the permeability of the porous medium promotes the flow.
- An increase in the angle of the channel gradually decreases the velocity.
- An increase in the Froude number initially opposes the flow, then gradually promotes it.
- The velocity shows mixed trends with Frequency and time since the motion is pulsating.
- At the lower plate of the channel, shear stress decreases initially, then increases

with the Froude number, decreases with the Hartmann number, increases with permeability, and decreases with inclination.

- At the upper plate of the channel, shear stress decreases initially, then increases with the Froude number, decreases rapidly, then slowly with the Hartmann number, increases slowly with permeability, and decreases slowly with inclination of the channel.

REFERENCES

[1] Malashetty, M. S., and Umavathi, J. C., (1997) *Two-phase magnetohydrodynamic flow and heat transfer in an inclined channel*, International Journal of Multiphase Flow, **23**, no. 3, 545–560.

[2] Ghosh, U., and Debnath, S.,(2019) *Numerical Simulation of Two-Phase Flow in an Inclined Porous Channel*, Advances in Applied Mathematics and Mechanics, **12**, no. 3, 345–360.

[3] Kumar, D., and Agarwal, M., (2017) *Flow of Two Immiscible Viscous Fluids in Porous Medium Between Two Parallel Plates*, GANITA, **67**, no. 1, 61–71.

[4] Umavathi, J. C., Chamkha, A. J., Mateen, A., and Al-Mudhaf, A.,(2009) *Unsteady Oscillatory Flow and Heat Transfer in a Horizontal Composite Porous Medium Channel*, Nonlinear Analysis: Modelling and Control, **14**, no. 3, 397–415.

[5] Abbas, Z., Hasnain, J., and Sajid, M., (2016) *MHD Two-Phase Fluid Flow and Heat Transfer with Partial Slip in an Inclined Channel*, Thermal Science, **20**, no. 5, 1435–1446.

[6] Chamkha, A. J., (2000) *Flow of Two-Immiscible Fluids in Porous and Nonporous Channels*, Journal of Fluids Engineering, **122**, no. 1, 117–124.

[7] Malashetty, M. S., Umavathi, J. C., and Prathap Kumar, J., (2004) *Two fluid flow and heat transfer in an inclined channel containing porous and fluid layer*, Heat and Mass Transfer, **40**, no. 11, 871–876.

[8] Priya, S. L., Govindarajan, A., and Sivakami, L., (2017) *Heat and mass transfer effect on MHD convective flow of immiscible fluid in a horizontal channel in the presence of chemical reaction and heat source*, International Journal of Pure and Applied Mathematics, **113** , no. 13, 252–261.

[9] Malashetty, M. S., and Leela, V.,(1992) *Magnetohydrodynamic heat transfer in two-phase flow*, International Journal of Engineering Science, **30**, no. 3, 371–377.

[10] Hanvey, R. R., Khare, R. K., and Paul, A.,(2017) *MHD Flow of Incompressible Fluid through Parallel Plates in Inclined Magnetic Field having Porous Medium with Heat and Mass Transfer*, International Journal of Scientific and Innovative Mathematical Research, **5**, no. 4, 18–22.

[11] Chamkha, A. J., Umavathi, J. C., and Mateen, A.,(2004) *Oscillatory Flow and Heat Transfer in Two Immiscible Fluids*, International Journal of Fluid Mechanics Research, **31** , no. 1, 13–36.

[12] Umavathi, J. C., Prathap Kumar, J., and Malashetty, M. S., (2001) *Convective Magnetohydrodynamic Two Fluid Flow and Heat Transfer in an Inclined Channel*, Heat and Mass Transfer, **37**, no. 2, 259–264.

[13] Hafeez, Y. H., and Ndikilar, C. E., (2014) *Flow of Viscous Fluid between Two Parallel Porous Plates with Bottom Injection and Top Suction*, Progress in Physics, **10** , no. 1, 49–51.

[14] Devi, M. P., and Srinivas, S.,(2023) *Heat transfer effects on the oscillatory MHD flow in a porous channel with two immiscible fluids*, Nonlinear Analysis: Modelling and Control, **28**, no. 3, 393–411.

[15] Umavathi, J. C., Chamkha, A. J., Mateen, A., and Al-Mudhaf, A., (2005) *Unsteady Two-Fluid Flow and Heat Transfer in a Horizontal Channel*, Heat and Mass Transfer, **42**, no. 2, 81–90.

[16] Xie, Fangfang, et al., (2017) *Direct numerical simulations of two-phase flow in an inclined pipe*, Journal of Fluid Mechanics, **825**, no. 4, 189–207.

[17] Yan, W. M., (1995) *Effects of wall transpiration on mixed convection in a radial outward flow inside rotating ducts*, International Journal of Heat and Mass Transfer, **38**, no. 13, 2333-2342.

Appendix

$C_1 = -\frac{A_8-A_9-A_{10}}{A_{11}+A_{12}-A_{13}-A_{14}}, C_2 = \frac{A_{15}(A_{16}+A_{17}-A_{18})}{A_{11}+A_{12}-A_{13}-A_{14}}, C_3 = \frac{A_{19}(A_{20}+A_{21}-A_{22})}{A_{23}-A_{24}+A_{25}+A_{26}}, C_4 = \frac{A_{27}+A_{21}-A_{28}}{A_{23}-A_{24}+A_{25}+A_{26}},$
$C_5 = -\frac{-A_5(A_{29}+A_{30})+A_{31}(A_{32}+A_{33})}{A_{31}(A_{34}+A_{35})-A_{36}(A_{29}+A_{30})}, C_6 = -\frac{A_{37}+A_{38}+A_{39}}{A_{40}-A_{41}}, C_7 = -\left(\frac{A_{45}(A_{42}-A_{43}+A_{44})}{A_{40}-A_{41}}\right), C_8 = -(\frac{A_{46}-A_{43}+A_{47}}{A_{40}-A_{41}}, A_1 = \frac{\sin\phi R_1 - Fr^2 P_s R_1}{M^2 Fr^2}, A_2 = \frac{R_2}{\sqrt{K}}, A_3 = \frac{K\left(\sin\phi R_2 - Fr^2 R_2 \alpha P_s\right)}{Fr^2 R_2^2}, A_4 =$

$\sqrt{M^2+i\omega R_1}$, $A_5 = \frac{R_1\alpha P_0}{A_4}$, $A_6 = \sqrt{\frac{R_2(i\omega K+R_2)}{K}}$, $A_7 = \frac{\alpha P_0 R_2}{A_6^2}$, $A_8 = e^{hM}M\beta A_1 - e^{hM+2A_2}M\beta A_1 + e^{M}A_1A_2$, $A_9 = e^{hM}A_1A_2 + e^{M+2A_2}A_1A_2 - e^{hM+2A_2}A_1A_2$, $A_{10} = e^{M}A_2A_3 + 2e^{M+A_2}A_2A_3 - e^{M+2A_2}A_2A_3$, $A_{11} = -e^{2M}M\beta - e^{2hM}M\beta$, $A_{12} = e^{2M+2A_2}M\beta + e^{2hM+2A_2}M\beta$, $A_{13} = e^{2M}A_2 + e^{2hM}A_2$, $A_{14} = e^{2M+2A_2}A_2 + e^{2hM+2A_2}A_2$, $A_{15} = e^{M+hM}$, $A_{16} = -e^{M}M\beta A_1 + e^{M+2A_2}M\beta A_1 - e^{M}A_1A_2$, $A_{17} = e^{hM}A_1A_2 - e^{M+2A_2}A_1A_2 + e^{hM+2A_2}A_1A_2$, $A_{18} = e^{hM}A_2A_3 + 2e^{hM+2A_2}A_2A_3 - e^{hM+2A_2}A_2A_3$, $A_{19} = e^{A_2}$, $A_{20} = -e^{2M}M\beta A_1 - e^{2hM}M\beta A_1 + 2A_{15}M\beta A_1$, $A_{21} = e^{2M}M\beta A_3 + e^{2hM}M\beta A_3 - e^{2M+A_2}M\beta A_3$, $A_{22} = e^{2hM+A_2}M\beta A_3 + e^{2M+A_2}A_2A_3 - e^{2hM+A_2}A_2A_3$, $A_{23} = e^{2M}M\beta + e^{2hM}M\beta$, $A_{24} = e^{2M+2A_2}M\beta A_2 - e^{2hM+2A_2}M\beta$, $A_{25} = e^{2M}A_2 - e^{2hM}A_2$, $A_{26} = e^{2M+2A_2}A_2 - e^{2hM+2A_2}A_2$, $A_{27} = e^{2M+A_2}M\beta A_1 - 2e^{M+hM+A_2}M\beta A_1 + e^{2hM+A_2}M\beta A_1$, $A_{28} = e^{2hM+A_2}M\beta A_3 + e^{2M}A_2A_3 - e^{2hM}A_2A_3$, $A_{29} = -e^{A_4}\left(-e^{-A_6}+e^{A_6}\right)\beta A_4$, $A_{30} = e^{A_4}\left(e^{-A_6}A_6+e^{A_6}A_6\right)$, $A_{31} = e^{hA_4}$, $A_{32} = -e^{A_6}\left(-e^{-A_6}+e^{A_6}\right)A_6A_7$, $A_{33} = \left(e^{-A_6}A_6+e^{A_6}A_6\right)\left(A_5-A_7+e^{A_6}A_7\right)$, $A_{34} = e^{-A_4}\left(-e^{-A_6}+e^{A_6}\right)\beta A_4$, $A_{35} = e^{-A_4}\left(e^{-A_6}A_6+e^{A_6}A_6\right)$, $A_{36} = -e^{hA_4}$, $A_{37} = -e^{hA_4}\beta A_4A_5 + e^{hA_4+2A_6}\beta A_4A_5 - e^{A_4}A_5A_6$, $A_{38} = e^{hA_4}A_5A_6 - e^{A_4+2A_6}A_5A_6 + e^{hA_4+2A_6}A_5A_6$, $A_{39} = e^{A_4}A_6A_7 - 2e^{A_4+A_6}A_6A_7 + e^{A_4+2A_6}A_6A_7$, $A_{40} = -e^{2A_4}\beta A_4 - e^{2hA_4}\beta A_4 + e^{2A_4+2A_6}\beta A_4 + e^{2hA_4+2A_6}\beta A_4$, $A_{41} = e^{2A_4}A_6 + e^{2hA_4}A_6 - e^{2A_4+2A_6}A_6 + e^{2hA_4+2A_6}A_6$, $A_{42} = e^{2A_4}\beta A_4A_5 + e^{2hA_4}\beta A_4A_5 - 2e^{A_4+hA_4}\beta A_4A_5$, $A_{43} = e^{2A_4}\beta A_4A_7 - e^{2hA_4}\beta A_4A_7 + e^{2A_4+A_6}\beta A_4A_7$, $A_{44} = e^{2hA_4+A_6}\beta A_4A_7 - e^{2A_4+A_6}A_6A_7 + e^{2hA_4+A_6}A_6A_7$, $A_{45} = e^{A_6}$, $A_{46} = -e^{2A_4+A_6}\beta A_4A_5 + 2e^{A_4+hA_4+A_6}\beta A_4A_5 - e^{2hA_4+A_6}\beta A_4A_5$, $A_{47} = e^{2hA_4+A_6}\beta A_4A_7 - e^{2A_4}A_6A_7 + e^{2hA_4}A_6A_7$